RSC Advances

PAPER

View Article Online
View Journal | View Issue

Cite this: *RSC Adv.*, 2019, **9**, 10825

Mechanistic insight into the self-coupling of 5-hydroxymethyl furfural to C_{12} fuel intermediate catalyzed by ionic liquids†

Jingjing Li,*[a] Binfen Wang,[a] Yefan Dou[a] and Yiying Yang[b]

Received 31st January 2019
Accepted 30th March 2019

DOI: 10.1039/c9ra00827f

rsc.li/rsc-advances

DFT calculations have been carried out to obtain insight into the self-coupling of biomass-based 5-hydroxymethyl furfural (HMF) to C_{12} fuel intermediate 5,5′-dihydroxymethyl furoin (DHMF) catalyzed by ionic liquids (ILs). It was found that acetate-based IL or thiazolium IL in combination with the additive Et_3N show high catalytic performance, wherein N-heterocyclic carbons (NHCs) derived from the cations of ILs act as the nucleophiles and the protonated acetate anion or the $[Et_3NH]^+$ acts as the proton shuttle. The effectiveness of this catalysis is attributed to the proton-shared three-center-four-electron (3c-4e) bonds between HMF and HOAc or $[Et_3NH]^+$, which stabilize the transition states and the intermediates. In addition, the results of the calculations also confirm that the nucleophilicity and basicity of NHCs are key factors for the self-coupling reaction. These results rationalize the experimental findings and offer valuable insights into understanding the catalysis of ILs.

1. Introduction

The utilization of biomass instead of nonrenewable fossil resources has become a hot topic.[1–3] Lignocellulose, a promising class of renewable and nonedible biomass resources has drawn significant attention as a carbon resource for generating value-added chemicals and high-quality fuel products.[4–6] Among them, 5-hydroxymethyl furfural (HMF) is considered as a versatile lignocellulose-derived platform molecule and can be transformed into small organic molecules, such as biofuel 2,5-dimethylfuran and 2,5-dihydroxymethylfuran.[7–9] More importantly, HMF can serve as a precursor for the production of 5,5′-dihydroxymethyl furoin (DHMF), a high energy-density C_{12} fuel intermediate that could be further converted into oxygenated diesels and alkane fuels.[10–12]

Dumesic *et al.* carried out the pioneering work of upgrading lignocellulose-derived C_5–C_6 molecules into larger fuel precursors ($C_{8–15}$ fuel intermediates) through aldol condensation.[10] Later, Huang *et al.*[13] studied the self-coupling of furfural (FF) and 5-methylfurfural to diesel fuel precursors (C_{10} and C_{12} fuel intermediates) by metal catalysts. Another attractive route for the biomass conversion is using environmentally benign and atom economical ionic liquids (ILs) as reaction media or catalysts,[14,15] which are characterized by unique properties, such as relatively low volatility, high thermal stability, nonflammability and excellent designability, through the modification of cations and anions.[16] Following the first application of ILs as efficient solvents and catalysts for the dissolution and fractionation of lignocellulose by the groups of Rogers and Zhao,[17,18] interest in ILs-promoted biomass conversion has increased continuously and rapidly over the past decades. For instance, Chen and co-workers[19] reported that DHMF could be catalytically produced in good yield (87% isolated or 98% determined by HPLC or NMR) from HMF using 1-ethyl-3-methylimidazolium acetate ([EMIM]OAc) as a catalyst at ambient atmosphere and 60–80 °C. Following this work, the same group found that FF and HMF can rapidly self-couple to form C_{10} and C_{12} furoins by using thiazolium ILs in combination with an additive organic base.[20] On the basis of the mechanism for the benzion condensation of benzaldehyde catalyzed by N-heterocyclic carbene (NHC),[21] the authors proposed a mechanism in which NHCs derived from acetate-based IL or thiazolium IL play important roles to facilitate the self-coupling of FF and HMF.

However, to the best of our knowledge, the molecular mechanism for the self-coupling of HMF to DHMF catalyzed by ILs has not yet been elucidated. Inspired by these experimental findings, in this paper, we focused on the exploration of the detailed reaction mechanism for the novel catalytic self-coupling reaction using density functional theory (DFT), from which we expect reveal (i) what are the crucial roles of the cation and anion of the IL or additive, (ii) whether the discrete NHCs (*i.e.*, TPT (1,3,4-triphenyl-4,5-dihydro-1*H*-1,2,4-triazol-5-ylidene) and I^{t}Bu (1,3-di-*tert*-butylimidazolin-2-ylidene)) are

[a]*College of Arts and Sciences, Shanxi Agricultural University, Taigu, Shanxi, 030801, P. R. China. E-mail: jjlisxau@qq.com*

[b]*Key Lab of Colloid and Interface Chemistry, Ministry of Education, Institute of Theoretical Chemistry, Shandong University, Jinan, 250100, P. R. China*

† Electronic supplementary information (ESI) available: For additional computational results and Cartesian coordinates of all optimized structures located in this work. See DOI: 10.1039/c9ra00827f

catalytically active for the conversion, and (iii) the effect of different substituents of the IL cation on the reactivity. We hope that the visual geometric and energetic information provided through DFT calculations will contribute to an in-depth understanding of the reaction mechanism and will provide guidance for the development of more efficient catalytic systems for biomass conversion.

2. Computational details

The calculations were carried out by using the popular B3LYP functional.[22,23] The 6-311++G(d,p) basis set was used for all atoms except for the Br atom, which was described by the effective core potentials (ECPs) of Hay and Wadt with the LanL2DZ double-valence basis set.[24,25] All of the geometries for the minima and transition states involved in the self-coupling reaction were first fully optimized in the gas phase without any symmetry constraints and then fully re-optimized in the solvent model based on the density (SMD) continuum solvent model.[26,27] Different solvents, such as 1,2-dichloroethane and THF, were chosen in the SMD geometry optimization. Frequency calculations were performed to identify all optimized structures as minima (zero imaginary frequencies) or first-order saddle points (one imaginary frequency) and to provide free energies at 298.15 K. Thus, the present work only reports the relative Gibbs free energies (in kcal mol^{-1}) obtained from the SMD calculations. Intrinsic reaction coordinate (IRC)[28,29] calculations were also carried out to verify that each transition state actually connects the desired minima. In addition, natural bond orbital (NBO) analyses[30] were performed to evaluate the molecular orbitals. All calculations were implemented with the Gaussian 09 software package.[31]

Localized orbital locator (LOL),[32] multi-center bond order (M-CBO),[33] electrostatic potential (ESP),[34] and Hirshfeld charge[35] were calculated by Multiwfn 3.3.8 [36] at the B3LYP/6-31G(d,p) level.

3. Results and discussion

3.1 Mechanism proposed by Chen and co-workers[19]

Based on the experimental results, Chen and co-workers[19] proposed a possible reaction mechanism for the acetate IL-catalyzed self-condensation process (Scheme 1) that included five sub-steps: (1) the proton transfer from imidazolium cation to the acetate anion of [EMIM]OAc to generate the catalyst NHC **I**, (2) nucleophilic attack on the carbonyl group of HMF by NHC **I** to afford a zwitterionic tetrahedral intermediate **II**, (3) the deprotonation of intermediate **II** by the acetate anion to form a Breslow intermediate **III′** [21] that is equivalent to the acyl anion intermediate **III**, (4) nucleophilic attack on the carbonyl group

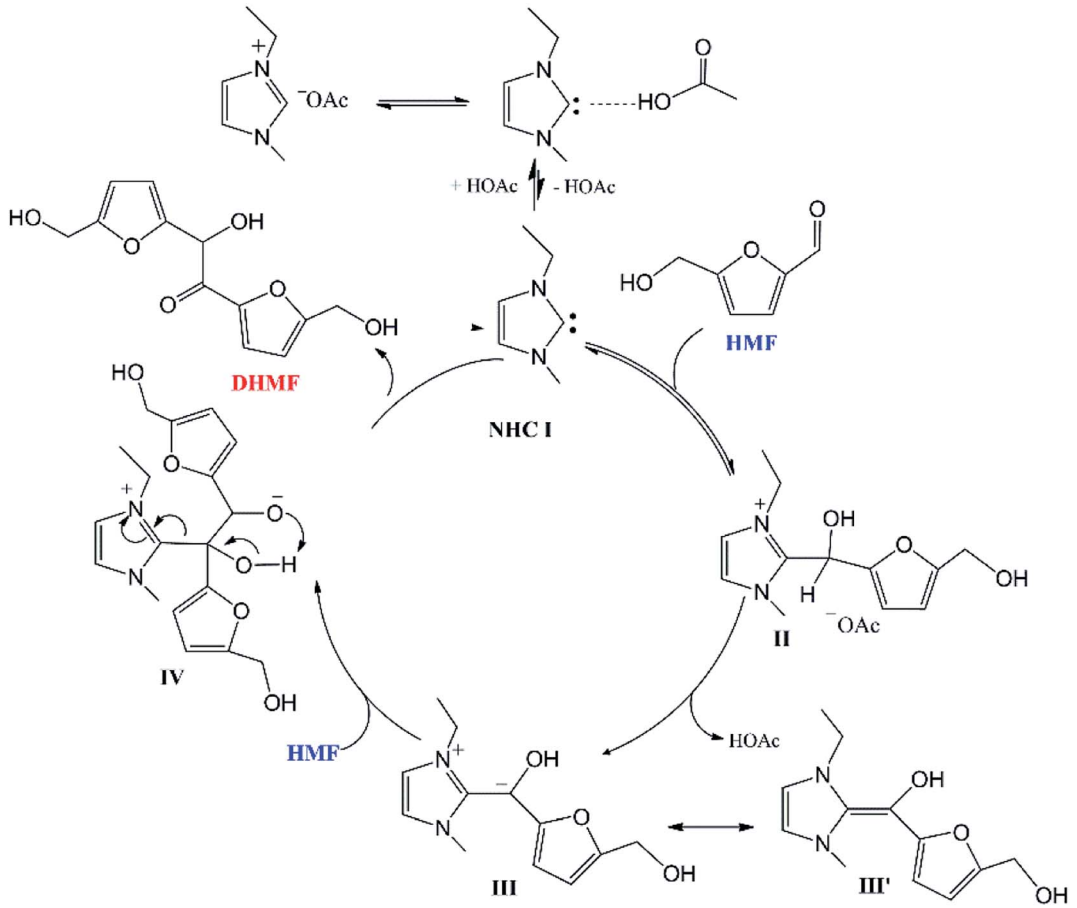

Scheme 1 Sketch of the catalytic cycle for the acetate IL-catalyzed self-coupling of HMF proposed by Chen and co-workers.[19]

of a second HMF molecule by intermediate **III** to give another tetrahedral intermediate **IV**, (5) intramolecular proton transfer and dissociation of NHC **I** leading to the production of DHMF.

3.2 Energetics and geometries associated with mechanism shown in Scheme 1

Here, we first provide detailed calculated results according to the catalytic cycle shown in Scheme 1. The calculated potential energy surface (PES) profile with schematic geometries of stationary points is displayed in Fig. 1.

The active species involved in the catalytic reaction is NHC **I**, and through our calculations, we found that proton transfer can easily occur from the imidazolium cation to the acetate anion of [EMIM]OAc by passing over a barrier of 9.0 kcal mol^{-1}, resulting in NHC **I**. After establishing the active NHC **I**, we now present the energetics and geometries associated with the mechanism shown in Scheme 1.

As illustrated in Fig. 1, the initial nucleophilic attack on the electrophilic carbonyl C atom of HMF by NHC **I** coupled with the proton transfer from HOAc to carbonyl O atom spans **TS1** with an energy barrier of 11.4 kcal mol^{-1}, affording a zwitterionic tetrahedral species **IM2**, which lies below the entrance by 10.7 kcal mol^{-1}. Subsequently, the deprotonation of **IM2** with the aid of the acetate anion *via* **TS2** requires surmounting a barrier of 19.3 kcal mol^{-1}, leading to a less stable acyl anion species **IM3**. With introducing a second HMF molecule and releasing of the HOAc from **IM3** give the intermediate **IM4**, which then again undergoes nucleophilic attack of the incoming carbonyl carbon of HMF, and accompanied by intramolecular proton transfer, furnishes another tetrahedral species **IM5**. The barrier for this step is 10.4 kcal mol^{-1} (the energy difference between **TS3** and **IM4**), which is nearly equal to the barrier for the first nucleophilic attack. Finally, the departure of NHC **I** to form the aimed product DHMF *via* **TS4** involves a notable barrier of 34.0 kcal mol^{-1}. The overall reaction is estimated to be exothermic by 0.2 kcal mol^{-1}.

To further understand the bonding interaction and electron distribution, the LOL profiles of **IM1**, **TS1** and **IM2** are presented in Fig. S1 in the ESI,† where a larger value indicates that more electrons are confined in this region and confirms the bond formation. Fig. S1(a) and (b)† depict the electron localization distributions in the C–C–O and C–O1–O plane, respectively. As shown in Fig. S1,† there is no C–C bonding interaction for **IM1**, and then the LOL value of C–C increased gradually, indicating the formation of the C–C bond. On the other hand, the LOL

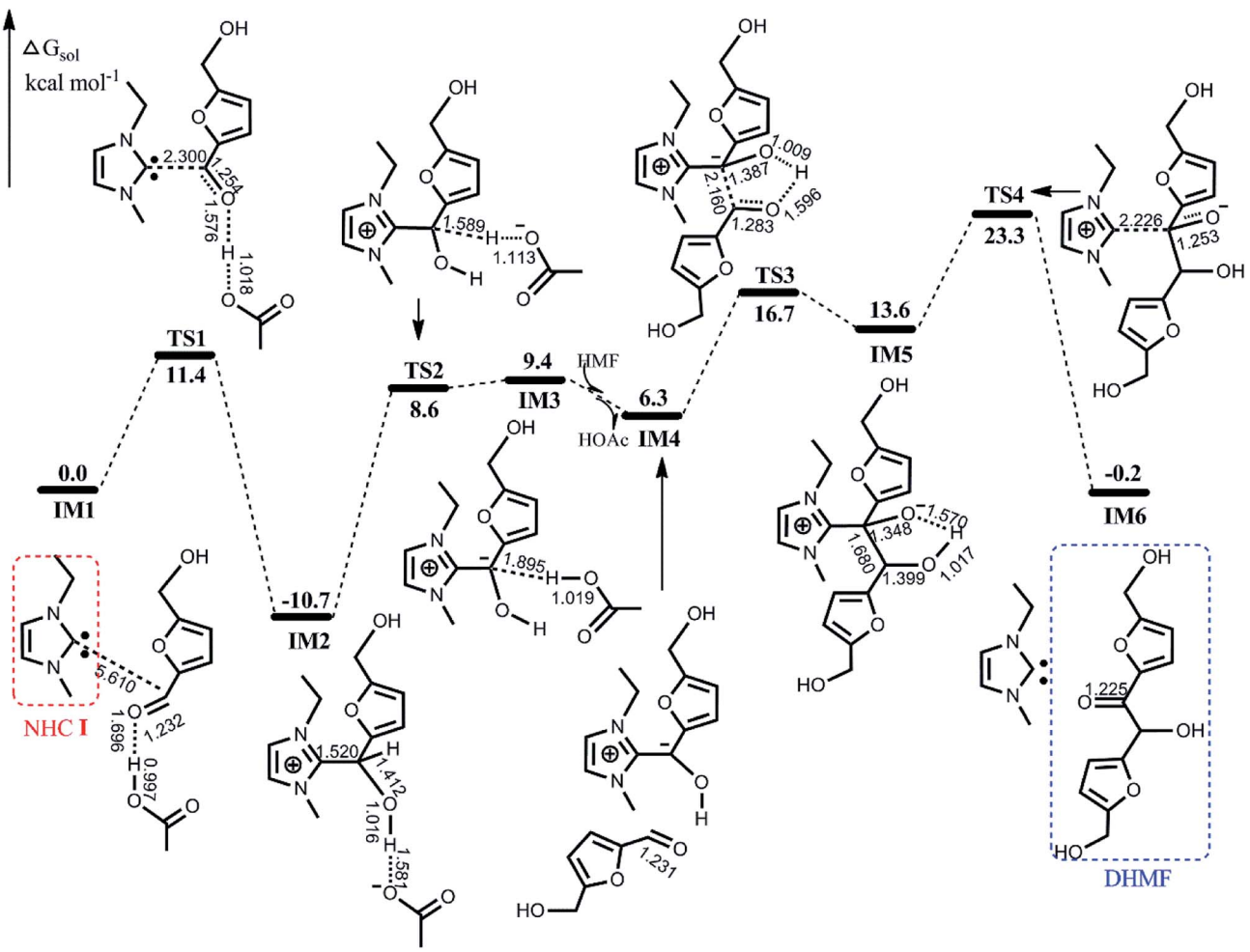

Fig. 1 Calculated free energy profile with schematic geometries according to the mechanism shown in Scheme 1. Bond distances are given in Å.

value of O–H decreased and that of H–O1 increased gradually along the reaction coordinate in Fig. S1(b),† demonstrating the proton shift between the O and O1 atoms.

On the basis of the discussion above, we conclude that the calculated barriers of the four sub-processes are 11.4, 19.3, 27.4 and 34.0 kcal mol^{-1}, respectively. Therefore, the final dissociation of NHC **I** is the bottleneck for the entire self-coupling process. This finding is qualitatively consistent with the experimental report that the first nucleophilic attack was conducted under mild conditions (60 °C) whereas the subsequent steps were carried out at an elevated temperature (80 °C). Furthermore, it is noteworthy that the zwitterionic tetrahedral species **IM2** is the most stable intermediate, which is in agreement with **IM2** observed experimentally.

3.3 Further discussion

3.3.1 Catalytic performance of [EMIM]Cl/DBU. As an acetate-based IL, [EMIM]OAc has been proved to play the roles of both NHC and "proton shuttle"[37] to promote the self-coupling of HMF, and therefore, we extend our study to investigate the catalytic performance of IL paired with a no-basic anion in combination with a strong organic base, such as [EMIM]Cl/DBU, to confirm whether such a combination would work in this kind of reaction. Our calculations showed that NHC **I** was easily obtained from the catalyst precursor [EMIM]Cl through the proton shift from the imidazolium cation to the sp^2-hybridized nitrogen of DBU by passing over a barrier of 9.9 kcal mol^{-1}. Understandably, with the exception of the first nucleophilic attack, the subsequent conversions are almost identical to those shown in Fig. 1. Therefore, we only located the pathway for the transformation from $\mathbf{IM1_{DBU}}$ to $\mathbf{IM2_{DBU}}$, as shown in Fig. 2. The barrier for this transformation is 14.8 kcal mol^{-1}, which is higher than that in Fig. 1 by 3.4 kcal mol^{-1}. This result indicates that as a proton shuttle, HOAc is more prominent than [DBUH]$^+$. To confirm this point, we analyzed the molecular orbitals and M-CBOs of relative structures.

$F^-\cdots H^+\cdots F^-$ (FHF) is a well-recognized three-center-four-electron (3c-4e) species. Fig. 3 compares the molecular orbitals and M-CBOs of $\mathbf{TS1_{DBU}}$, **TS1** and **IM1** with those of FHF. It is observed that both O$\cdots$H–N in $\mathbf{TS1_{DBU}}$ and O$\cdots$H–O in **TS1** have similar molecular orbitals to that of FHF, whereas the M-CBO (−0.044) of the later is closer to that (−0.103) of FHF than that of the former (−0.035), indicating that O$\cdots$H–O in **TS1** possess a large similarity to the 3c-4e bond in the FHF species. Such a 3c-4e bond may be mainly responsible for stabilizing the transition state structure, which is in agreement with the energy barrier calculated above. In addition, similar 3c-4e bond and M-CBO (−0.051) can be found in **IM2**, providing a reasonable explanation for the experimental detection of **IM2**.

3.3.2 Catalytic performance of discrete NHCs (TPT and I^{t}Bu). To further confirm the crucial role of the 3c-4e bond in promoting the self-coupling reaction, our calculations were extended to the cases where discrete NHCs (TPT and I^{t}Bu), in the absence of acetate or DBU, were applied as catalysts. The calculated relative free energies and optimized geometries of the critical structures are summarized in Table 1 and Fig. S2 in the ESI.† Compared with the energy of $\mathbf{TS1_R}$, and **TS1** in Fig. 1 and with the energy of $\mathbf{TS1_{DBU}}$ in Fig. 2, it can be clearly seen

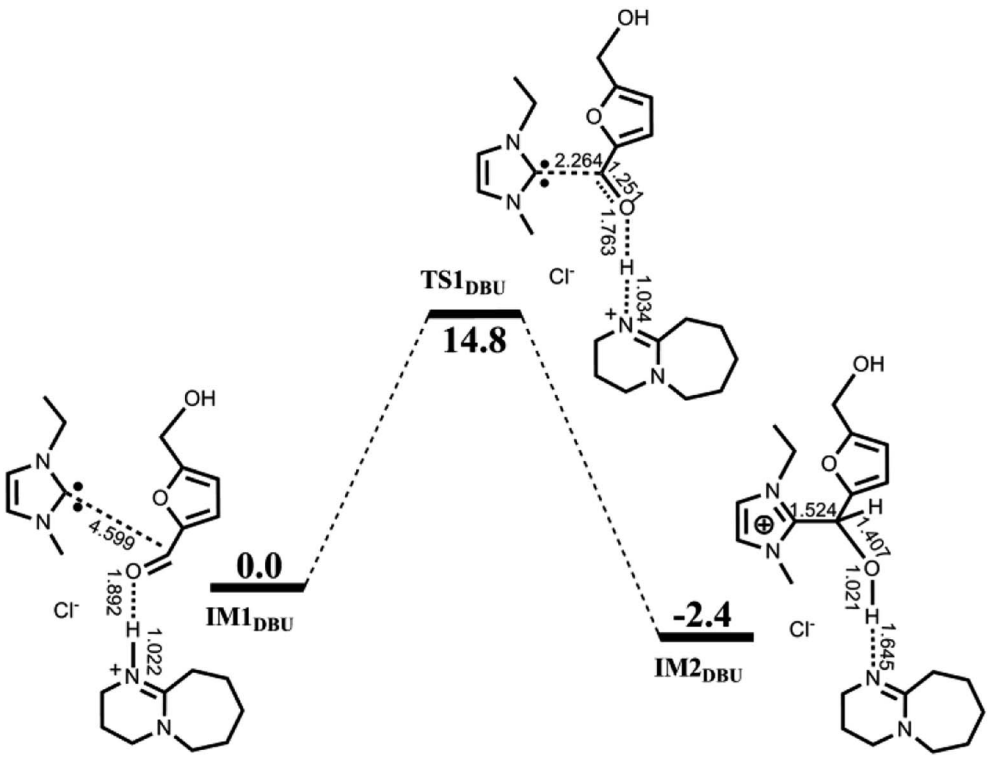

Fig. 2 Calculated free energy profile with schematic structures for the first nucleophilic attack catalyzed by [EMIM]Cl/DBU. Bond distances are given in Å.

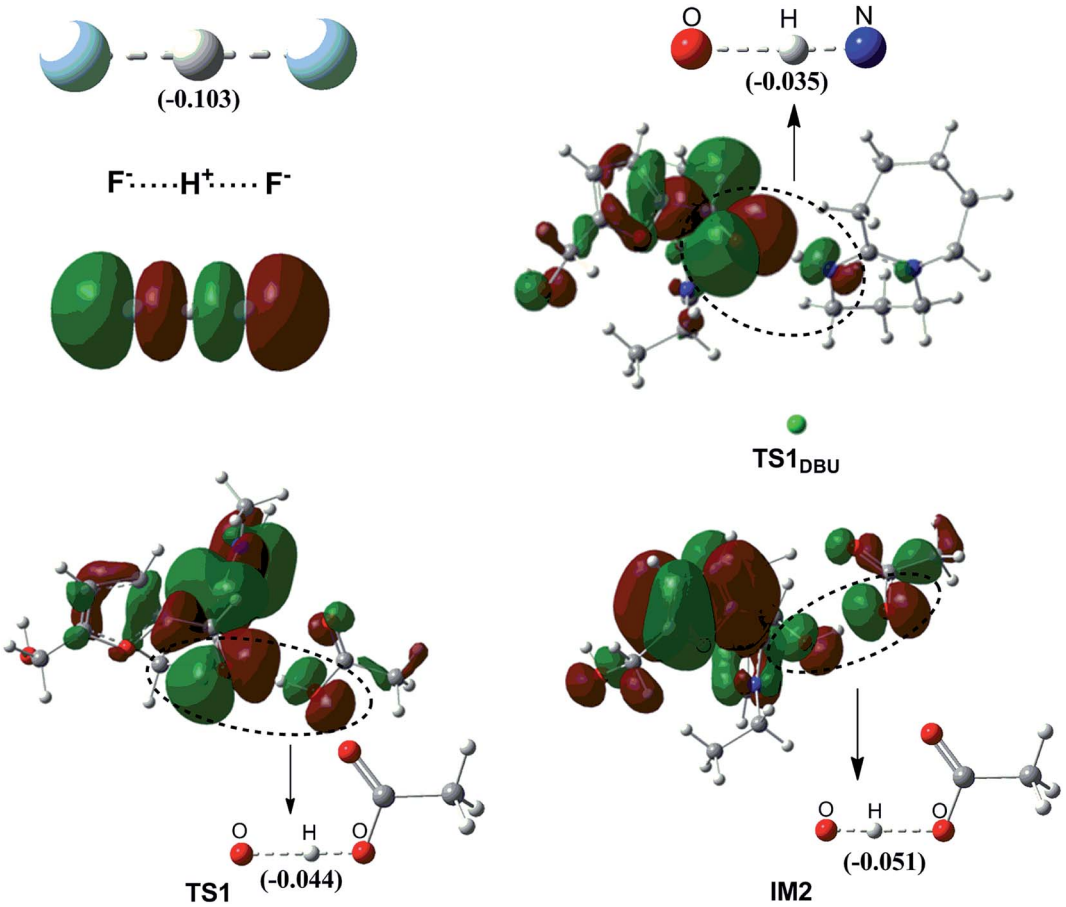

Fig. 3 The molecular orbitals and M-CBOs (in brackets) of $TS1_{DBU}$, TS1 and IM2 in comparison with $F^{-}\cdots H^{+}\cdots F^{-}$, a well-recognized 3c-4e bonding species.

that the transition states are significantly destabilized in the absence of 3c-4e bonds. Moreover, the rate-determining barriers calculated for the discrete NHCs-catalyzed systems are as high as 40.7 and 55.0 kcal mol^{-1}, respectively, which is again consistent with experimental observations that no product was obtained when TPT or I^{t}Bu were mixed with a stoichiometric amount of HMF.

3.3.3 Catalytic performance of thiazolium ILs. Interestingly, experiments show that thiazolium IL carrying an electron-donating group on the ring, 3-benzyl-5-(2-acetoxyethyl)-4-methylthiazolium chloride (^{AcO}[TM]Cl), was highly superior to 3-methyl-5-methoxycarbonyl-4-methylthiazolium iodine (^{Ac}[TM]I) bearing the electron-withdrawing group. To explore the substituent effects, in the following, we discuss the self-coupling mechanism for thiazolium ILs in combination with the additive Et_3N, and the results are collected in Fig. 4. Since the intrinsic mechanism is very similar to that shown in Fig. 1, we only present the first nucleophilic attack and last rate-determining step in Fig. 4. Both NHC **II** and NHC **III** shown in Fig. 4 are generated by the proton transfer from ^{AcO}[TM]Cl and ^{Ac}[TM]I to Et_3N. The energy barrier of the first nucleophilic attack is 9.3 kcal mol^{-1} for the NHC **II**-catalyzed system, while the calculated energy barrier is 11.0 kcal mol^{-1} for the NHC **III**-catalyzed system. More obviously, the rate-determining free energy barrier of the former is 4.2 kcal mol^{-1} lower than that found in the latter, which is in agreement with the experimental report.

Table 1 Relative free energies of the critical structures when discrete NHCs (TPT and I^{t}Bu) were applied as catalysts

	$IM1_R$	$TS1_R$	$IM2_R$	$IM5_R$	$TS4_R$	$IM6_R$
R = TPT	0.0	23.9	19.9	37.1	40.7	7.1
R = I^{t}Bu	0.0	29.4	23.0	47.3	55.0	7.1

The lower energy required for the NHC **II**-catalyzed system can be understood by examining the key structural details involved. As depicted in Fig. 5, the nucleophilicity of NHC **II** and NHC **III** are measured by ESP and Hirshfeld charge, which are usually used to predict the order of reactivity.[35] The negative electrostatic potential region is identified as a favorable site for a nucleophilic attack. The ESP results show that the global minima on the surfaces of NHC **II** and NHC **III** are −49.9 and −43.6 kcal mol^{-1}, respectively. On the other hand, the divalent carbon (0) of the latter has a larger Hirshfeld charge value than that of the former. Both of these results indicate that the nucleophilicity of NHC **II** is stronger than of NHC **III**. In addition, the presence of a more pronounced 3c-4e bonding structure in **TS1a** (see Fig. S3 in the ESI†) can also be responsible for the lower energy barrier. For the last rate-determining step, **TS4a** is lower than **TS4b** because the basicity of NHC **II** is weaker than that of NHC **III**. To confirm this point, we can compare the

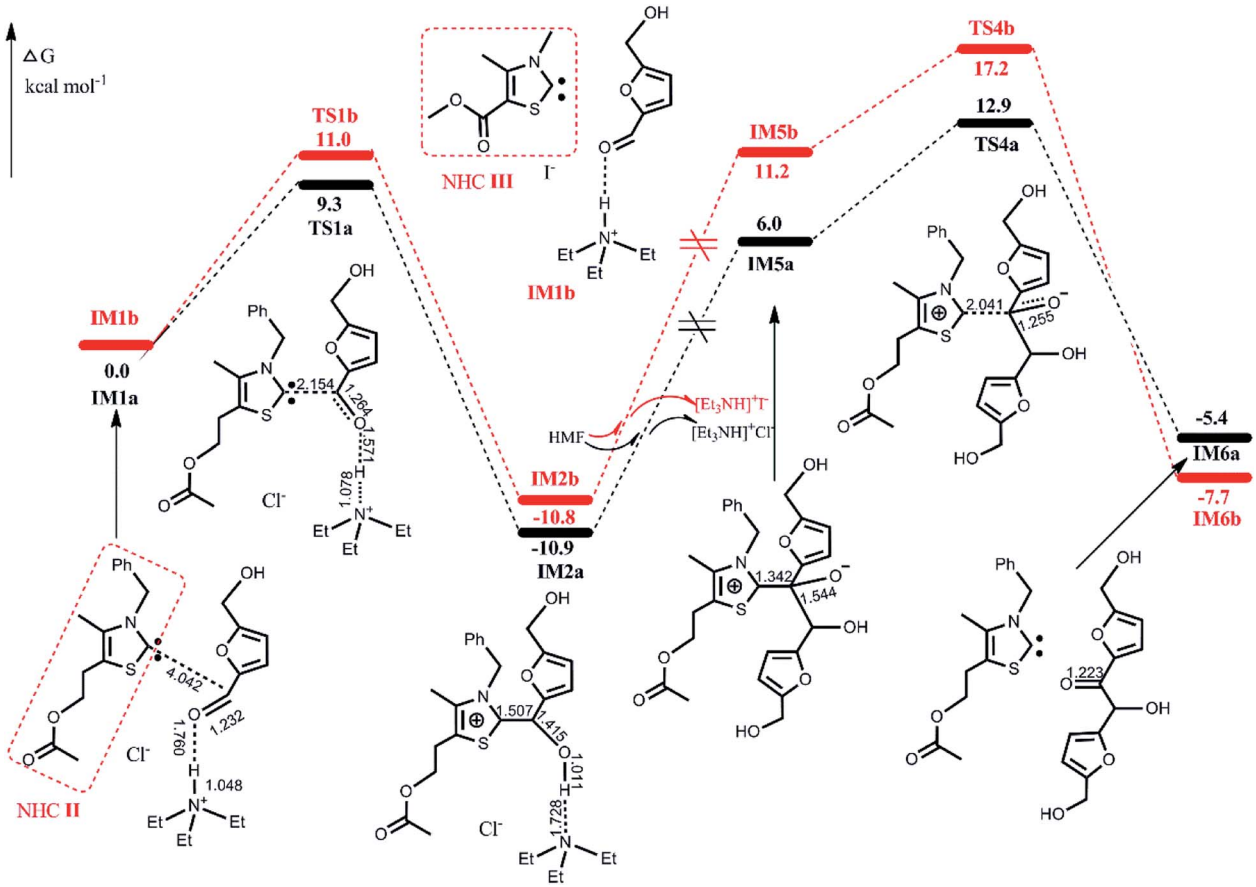

Fig. 4 Calculated free energy profiles with schematic structures for the first nucleophilic attack and last rate-determining step catalyzed by ^{AcO}[TM]Cl/Et$_3$N (black line) and ^{Ac}[TM]I/Et$_3$N (red line). The symbol of inequality sign denotes the pathway for the conversion from **IM2a** (**IM2b**) to **IM5a** (**IM5b**) has been omitted. Bond distances are given in Å.

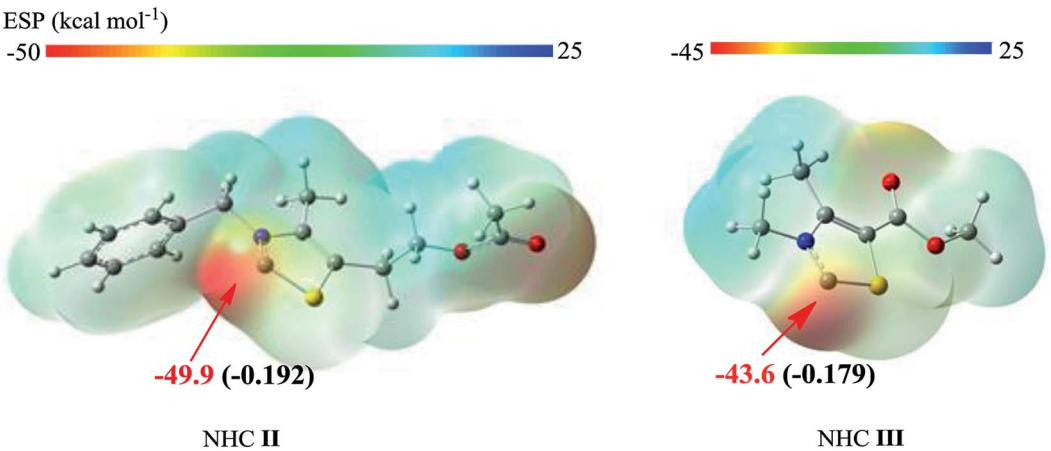

Fig. 5 ESP on the van der Waals surface of NHC **II** and NHC **III**. Surface local minima and maxima of ESP are represented as red and blue spheres, respectively. Only the global minima are labeled. The values in parentheses are calculated Hirshfeld charges.

acidity of their conjugate acids. The barriers for the deprotonation of ^{AcO}[TM]Cl and ^{Ac}[TM]I are 13.5 and 15.0 kcal mol^{-1}, respectively, suggesting that the former is more acidic, and in turn, its conjugate base (NHC **II**) is less basic. Taken together, these results show that NHC **II** is not only a strong nucleophile but also a good leaving group.

4. Conclusions

In summary, molecular insights into the self-coupling of HMF catalyzed by ILs were proposed with the aid of DFT calculations. After establishing the active NHC *via* proton transfer, the reaction undergoes four elementary steps, namely, the initial

nucleophilic attack, the deprotonation, the second nucleophilic attack accompanied by proton migration and finally, the dissociation of NHC. Computational results confirm that the last step is the rate-determining step. Analysis of molecular orbital and M-CBO demonstrate that the effectiveness of the acetate-based IL [EMIM]OAc and the thiazolium IL ^{AcO}[TM]Cl/Et_3N are attributed to the formation of proton-shared 3c-4e bonds between HMF and HOAc or $[Et_3NH]^+$. This is a reason for the remarkable stability of the zwitterionic tetrahedral intermediate. In addition, substituent effects were also taken into account to explain the experimental results and further confirmed that the nucleophilicity and basicity of NHCs are critical factors for the self-coupling reaction. The present theoretical results have not only rationalized the experimental findings well but also provide in-depth insight into the catalysis of ILs, which will be enlighten about the rational design of catalysts used in biomass conversion chemistry.

Conflicts of interest

The authors declare no conflict of interests.

Acknowledgements

This research was financially supported by PhD Research Startup Foundation of Shanxi Agricultural University, China (No. 2017YJ37) and Excellent PhD Award to Work in Shanxi Province of China (No. SXYBKY201724).

Notes and references

1 C. O. Tuck, E. Perez, I. T. Horvath, R. A. Sheldon and M. Poliakoff, *Science*, 2012, **337**, 695–699.
2 A. J. J. Straathof, *Chem. Rev.*, 2014, **114**, 1871–1908.
3 M. Besson, P. Gallezot and C. Pinel, *Chem. Rev.*, 2014, **114**, 1827–1870.
4 A. Rahimi, A. Ulbrich, J. J. Coon and S. S. Stahl, *Nature*, 2014, **515**, 249–252.
5 Z. Zhang, J. Song and B. Han, *Chem. Rev.*, 2017, **117**, 6834–6880.
6 L. T. Mika, E. Cséfalvay and Á. Németh, *Chem. Rev.*, 2018, **118**, 505–613.
7 M. Chatterjee, T. Ishizaka and H. Kawanami, *Green Chem.*, 2014, **16**, 1543–1551.
8 M. Chidambaram and A. T. Bell, *Green Chem.*, 2010, **12**, 1253–1262.
9 L. Hu, J. Xu, S. Zhou, A. He, X. Tang, L. Lin, J. Xu and Y. Zhao, *ACS Catal.*, 2018, **8**, 2959–2980.
10 G. W. Huber, J. N. Chheda, C. J. Barrett and J. A. Dumesic, *Science*, 2005, **308**, 1446–1450.
11 Y. Román-Leshkov, C. J. Barrett, Z. Y. Liu and J. A. Dumesic, *Nature*, 2007, **447**, 982–986.
12 D. M. Alonso, J. Q. Bond and J. A. Dumesic, *Green Chem.*, 2010, **12**, 1493–1513.
13 Y. Huang, Z. Yang, J. Dai, Q. Guo and Y. Fu, *RSC Adv.*, 2012, **2**, 11211–11214.
14 J. P. Hallett and T. Welton, *Chem. Rev.*, 2011, **111**, 3508–3576.
15 X. Kang, X. Sun and B. Han, *Adv. Mater.*, 2016, **28**, 1011–1030.
16 A. S. Amarasekara, *Chem. Rev.*, 2016, **116**, 6133–6183.
17 R. P. Swatloski, S. K. Spear, J. D. Holbrey and R. D. Rogers, *J. Am. Chem. Soc.*, 2002, **124**, 4974–4975.
18 H. Zhao, J. E. Holladay, H. Brown and Z. Zhang, *Science*, 2007, **316**, 1597–1600.
19 D. Liu, Y. Zhang and E. Y. X. Chen, *Green Chem.*, 2012, **14**, 2738–2746.
20 H. Zang and E. Y. X. Chen, *Int. J. Mol. Sci.*, 2015, **16**, 7143–7158.
21 R. Breslow, *J. Am. Chem. Soc.*, 1958, **80**, 3719–3726.
22 A. D. Becke, *J. Chem. Phys.*, 1993, **98**, 5648–5652.
23 B. Miehlich, A. Savin, H. Stoll and H. Preuss, *Chem. Phys. Lett.*, 1989, **157**, 200–206.
24 P. J. Hay and W. R. Wadt, *J. Chem. Phys.*, 1985, **82**, 270–283.
25 W. R. Wadt and P. J. Hay, *J. Chem. Phys.*, 1985, **82**, 284–298.
26 A. V. Marenich, C. J. Cramer and D. G. Truhlar, *J. Phys. Chem. B*, 2009, **113**, 6378–6396.
27 V. S. Bernales, A. V. Marenich, R. Contreras, C. J. Cramer and D. G. Truhlar, *J. Phys. Chem. B*, 2012, **116**, 9122–9129.
28 V. Barone and M. Cossi, *J. Phys. Chem. A*, 1998, **102**, 1995–2001.
29 K. Fukui, *Acc. Chem. Res.*, 1981, **14**, 363–368.
30 A. E. Reed, L. A. Curtiss and F. Weinhold, *Chem. Rev.*, 1988, **88**, 899–926.
31 M. J. Frisch, G. W. Trucks, H. B. Schlegel, G. E. Scuseria, M. A. Robb, J. R. Cheeseman, G. Scalmani, V. Barone, B. Mennucci, G. A. Petersson, H. Nakatsuji, M. Caricato, X. Li, H. P. Hratchian, A. F. Izmaylov, J. Bloino, G. Zheng, J. L. Sonnenberg, M. Hada, M. Ehara, K. Toyota, R. Fukuda, J. Hasegawa, M. Ishida, T. Nakajima, Y. Honda, O. Kitao, H. Nakai, T. Vreven, J. A. Montgomery Jr, J. E. Peralta, F. Ogliaro, M. Bearpark, J. J. Heyd, E. Brothers, K. N. Kudin, V. N. Staroverov, R. Kobayashi, J. Normand, K. Raghavachari, A. Rendell, J. C. Burant, S. S. Iyengar, J. Tomasi, M. Cossi, N. Rega, J. M. Millam, M. Klene, J. E. Knox, J. B. Cross, V. Bakken, C. Adamo, J. Jaramillo, R. Gomperts, R. E. Stratmann, O. Yazyev, A. J. Austin, R. Cammi, C. Pomelli, J. W. Ochterski, R. L. Martin, K. Morokuma, V. G. Zakrzewski, G. A. Voth, P. Salvador, J. J. Dannenberg, S. Dapprich, A. D. Daniels, Ö. Farkas, J. B. Foresman, J. V. Ortiz, J. Cioslowski and D. J. Fox, *Gaussian 09 Revision B.01*, Gaussian, Inc., Wallingford, CT, 2009.
32 H. L. Schmider and A. D. Becke, *J. Mol. Struct.: THEOCHEM*, 2000, **527**, 51–61.
33 T. Lu and S. Manzetti, *Struct. Chem.*, 2014, **25**, 1521–1533.
34 J. Liu, J. Wu, J. Zhu, Z. Wang, J. Zhou and K. Cen, *Fuel*, 2016, **178**, 85–92.
35 J. Cao, Q. Ren, F. Chen and T. Lu, *Sci. China: Chem.*, 2015, **58**, 1845–1852.
36 T. Lu and F. Chen, *J. Comput. Chem.*, 2012, **33**, 580–592.
37 Y. Xia, Y. Liang, Y. Chen, M. Wang, L. Jiao, F. Huang, S. Liu, Y. Li and Z. Yu, *J. Am. Chem. Soc.*, 2007, **129**, 3470–3471.